ORIGINAL PAPER

physica status solidi a
www.pss-a.com

Fabrication of Nanopillars on Nanocrystalline Diamond Membranes for the Incorporation of Color Centers

*Alexander Schmidt, Josselin Bernardoff, Kilian Singer, Johann P. Reithmaier, and Cyril Popov**

A fabrication process of dense arrays of one-dimensional diamond nanostructures (diamond nanopillars) integrated on nanocrystalline diamond (NCD) membranes is implemented with an etched-through marker hole in the membrane in the center of the array. NCD films deposited on silicon substrates are used as starting material. The main fabrication steps consist of structuring the NCD film by electron beam lithography (EBL) applying aluminum as a hard mask and subsequent inductively coupled O_2 plasma reactive ion etching (ICP RIE), followed by structuring of the silicon substrate from the backside to open a NCD membrane. The developed fabrication procedure for nanostructured membranes can be transferred to monocrystalline diamond and implemented for deterministic single ion implantation into the nanopillars for generation of nitrogen-vacancy (NV) or silicon-vacancy (SiV) centers. For this purpose, the etched marker hole can be applied for alignment in the implantation process. Such diamond nanostructures with integrated color centers could play an important role in the development of novel quantum memory devices.

1. Introduction

In the last decade there has been an ever-increasing scientific interest regarding different colors centers in diamonds crystal lattice and their outstanding properties. Therefore, novel applications for components in quantum information technologies (QIT) like quantum memories and processors, quantum repeaters or single photon sources based on colors centers in diamond can be envisioned.[1–3] Two promising luminescent diamond lattice defects are the nitrogen-vacancy (NV) and the silicon-vacancy (SiV) centers. The former is composed of a nitrogen atom substituting a carbon atom adjacent to a vacancy in the diamond lattice, whereas the latter consists of a silicon atom between two vacant lattice sites. Such defects may be considered as "artificial atoms" in the solid state, since they can be embedded and processed into solids by means of modern fabrication techniques and demonstrate quantum mechanical properties of single atoms.[4] In particular, the negatively charged NV centers have been thoroughly studied, showing distinctive electron spin properties including an easy initialization, manipulation (e.g. with microwaves) and readout, and long spin decoherence T_2 times up to the millisecond range at room temperature.[5,6] However, the NV center exhibits phonon-broadened emission spectra and only a few percent of the photons are emitted in the zero-phonon line (ZPL) at 637 nm.[7] In contrast, the SiV center shows a weak phonon side band, a sharp ZPL at 738 nm and very short photoluminescence lifetimes of 1–4 ns.[8]

The collection efficiency of the emitted photons can be enhanced to achieve maximum fluorescence output by incorporation of the color centers into optical cavities, e.g. in diamond nanopillars,[9–12] photonic crystals,[13] microrings,[14] microdisks,[15] nanobeam photonic crystal cavities[16] etc. According to calculations and measurements, color centers integrated in diamond nanopillars with a diameter of ca. 200 nm have shown the maximum fluorescence intensities.[10]

There are different approaches to create NV or SiV centers: i) N or Si ion implantation into the diamond, which additionally creates vacancies along the implantation tracks, followed by an annealing step in order to promote the migration of the vacancies to the substitutional implanted ions in the lattice.[17–19] ii) in situ doping during the diamond growth by introducing precursor gas mixtures into the reaction chamber, e.g. Si containing gases like SiH_4 for the creation of SiV centers[20] or nitrogen gas for the formation of NV centers: either in a controlled way for nanometer-precision depth control of the generated NV centers (delta-doping)[21] or distributed within the diamond film by a background pressure of nitrogen in the chamber.[22] In the case of SiV centers, also solid precursor sources are possible, e.g. a silicon substrate or a piece of silicon, which are positioned close to the diamond sample and etched in a hydrogen containing plasma to incorporate silicon atoms

A. Schmidt, Prof. J. P. Reithmaier, Prof. C. Popov
Institute of Nanostructure Technologies and Analytics
Center of Interdisciplinary Nanostructure Science and Technology (CINSaT)
University of Kassel
Heinrich-Plett-Str. 40, D-34132 Kassel, Germany
E-mail: popov@ina.uni-kassel.de

J. Bernardoff, Prof. K. Singer
Institute of Physics
Center of Interdisciplinary Nanostructure Science and Technology (CINSaT)
University of Kassel
Heinrich-Plett-Str. 40, D-34132 Kassel, Germany

DOI: 10.1002/pssa.201900233

during the deposition.[23] Beside conventional ion implantation, also novel deterministic single ion implantation methods have been recently realized. With such techniques implantation with nanometer accuracy for the creation of single color centers (SiV or NV) into individual nanostructures for the fabrication of scalable novel quantum technology devices and components can be envisioned.[24–27]

In this study we demonstrate the implementation of a fabrication process for nanocrystalline diamond (NCD) membranes with integrated arrays of nanopillars and completely etched marker holes in the center of the arrays. Therefore, NCD films deposited on silicon wafers have been used as starting material. We have transferred and optimized our established fabrication method for single diamond nanopillars[22] to highly dense arrays of nanopillars. Proximity correction software of electron beam lithography (EBL) and exposure dose variations were included for realization of closely packed features. Afterwards our "top-down" fabrication process was followed by metal mask deposition, lift-off and inductively coupled plasma reactive ion etching (ICP RIE) with oxygen. In addition, marker holes were implemented into the fabrication process by the same techniques, precisely aligned to the pillar arrays via EBL. After lithographic structuring of the backside of the sample, wet chemical etching in KOH was used to remove the silicon substrate under the nanostructures and to suspend a NCD membrane. The fabrication procedure can be adjusted and transferred to monocrystalline diamond membranes, which have been already demonstrated by several groups using ion implantation and lift-off processes.[28–30] In this way nanostructured monocrystalline diamond membranes with a thickness of ca. 300 nm could be achieved. In addition, thin monocrystalline diamond plates (20–50 μm) have become commercially available and "top-down" approaches using reactive ion etching for further thinning down have been demonstrated successfully fabricating high quality nanostructured monocrystalline diamond membranes.[31–33] By incorporating arrays of nanopillars with a marker hole on monocrystalline diamond membranes, such nanostructures could be used not only for deterministic implantation of single ions in order to generate color centers (single or ensembles of NV or SiV) for the creation of scalable quantum devices (e.g. qubits, dense emitter arrays) but also for photonic crystals. Diamond nanopillar array photonic crystal cavities have been already demonstrated specifically enhancing the emission from near-surface NV centers[34] as well as bottom-up engineered photonic crystal slabs enhancing the emission extraction (up to 14-fold) of SiV centers.[35]

2. Results and Discussions

Arrays of pillars with nominal diameters of 200 nm and center-to-center distances of 400 nm with completely etched marker holes in the center of the array were fabricated on a NCD membrane following the workflow shown in **Figure 1**. The starting material was closed NCD films with a thickness of ca. 3 μm exhibiting well-facetted topography with crystallite sizes in the sub-micron range, as revealed by the SEM micrographs (**Figure 2**). The structured nanopillars include parts of several crystals as shown by scanning transmission electron microscopy

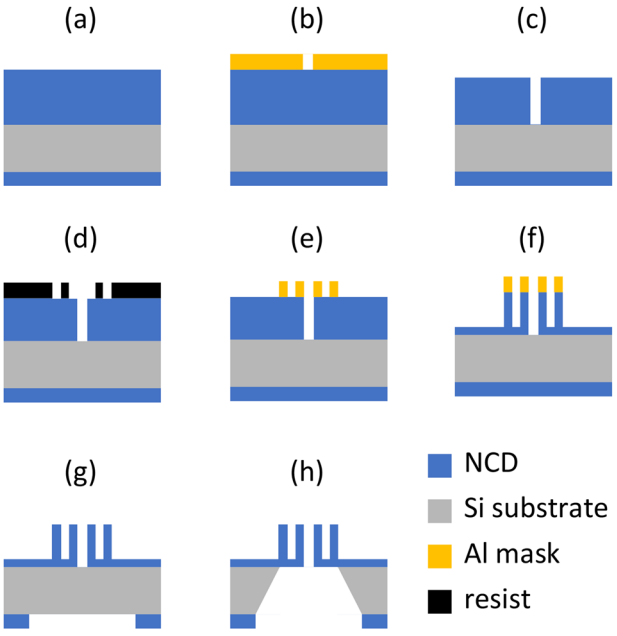

Figure 1. Workflow of the fabrication process of nanostructured nanocrystalline diamond membranes: a) starting material; b) 1st structuring step including electron beam lithography (EBL), Al mask deposition and lift-off; c) inductively coupled O_2 plasma reactive ion etching (ICP RIE); d) 2nd successively aligned EBL; e) Al mask deposition and lift-off; f) ICP RIE; g) 3rd successively aligned lithography from the backside, followed by Al mask deposition, lift-off and ICP RIE; h) anisotropic wet etching in KOH.

in a former paper.[23] Images of the membrane windows and nanopillar arrays with a marker hole prepared in the current work from the NCD films can be seen in **Figure 3**. The shape of the pillars was well defined and quite homogeneous throughout the entire array as can be seen in Figure 3. Proximity correction software and exposure dose variations in the EBL step were used to achieve the best fidelity of the pattern design. The best results were obtained with a base exposure dose of 21 μC cm^{-2} and its distribution as shown in Figure 3d.

The average top diameter (198 ± 3) nm of the pillars was very close to the defined nominal value. However, a slightly tapering character of the top parts of the pillars can be seen in Figure 3, as well as some irregularities in the circular shapes of the pillars (Figure 3b). Several effects could play a role affecting the final shape of the pillars: i) since NCD is not conductive, charging effects can occur during EBL deflecting the electron beam and deforming the defined circles; ii) surface roughness; especially as-grown unplanarized NCD samples with high surface roughness had significant deformations of the circular shape; iii) mask erosion during the dry etching in the ICP RIE step.

The pillars at the edge of an array were slightly stronger etched than the pillars surrounding the center, which can be seen by comparing their sidewalls in Figure 3. Those at the edge were more tapered, however this effect is far less pronounced compared to a previous study,[22] where we investigated single nanopillars separated by five micrometers and the top diameters were significantly smaller than the bottom ones showing

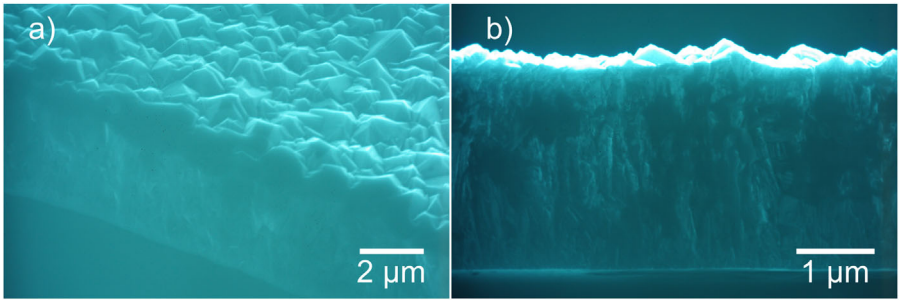

Figure 2. SEM micrographs of the starting diamond films under a tilting angle of 45° (a) and 90° (b).

pronounced tapering. This could be explained by the higher package density of the pillars in the current study: Their overall exposure to the plasma in the ICP RIE step is limited which reduces overetching and mask erosion. Additionally, this can explain the slight differences of the sidewall angles between pillars at the edge and the center of the array.

The pillars situated directly at the rim of the marker hole were damaged because of the inherent proximity of both structures, however, the loss of pillars was only minimal. The top diameter of the hole was about 1.9 µm, close to the defined 2 µm. However, its bottom diameter was only about 1.3 µm, indicating a tapering of the sidewall, which is clearly visible in Figure 3b. It can be assumed that this tapering stems from the relatively deep RIE of the complete diamond film.

It has to be noted that various sequences of the individual technological steps of the fabrication process were tested. It was not possible to open the NCD membranes first and subject them afterwards to EBL even though they could be subjected to spin-coating without vacuum fixation directly below the membrane. The electron sensitive resist showed no response exclusively at the membrane windows. One reason could be the missing silicon substrate reducing in such a way the conductivity or heat transfer for the baking of the resist.

The last fabrication step (Figure 1h) had to be performed with the nanostructured pillars facing down and the blank silicon windows facing up, otherwise vigorous bubbling from the reaction of the silicon with KOH would destroy the membrane.

In general, the stability of the membrane can be adjusted by its size and thickness. We found a good compromise between

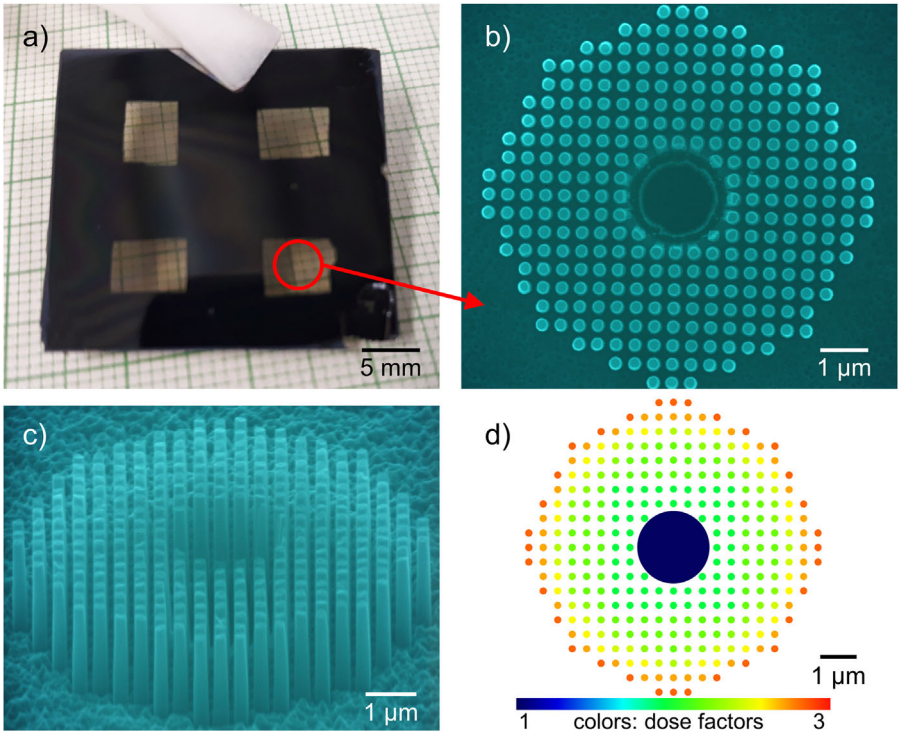

Figure 3. a) Photo of a fully structured sample with four NCD membranes (1.5 µm thick). SEM (b) top view and (c) side view under a tilting angle of 70° images of a NCD nanopillar array integrated on a membrane. Note that the hole in the center is completely etched through the membrane. d) Schematic diagram of proximity corrections to the pattern design (For colors please see online version).

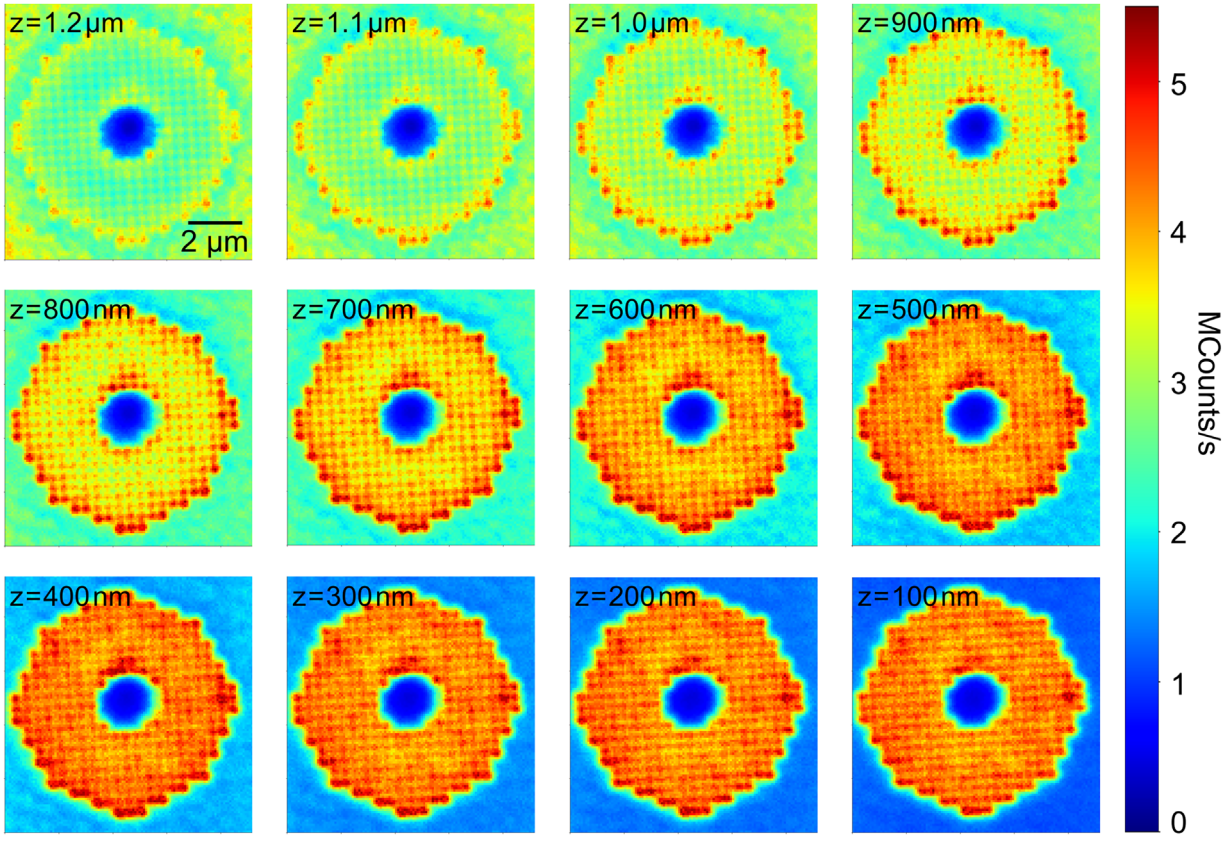

Figure 4. Fluorescence maps of different focal planes along the z-axis of an array. The scan starts on the top left image, focused in the diamond membrane and ends on the bottom right image, focused in the nanopillars. The arbitrary focus depth is depicted on each image (For colors please see online version).

stability and easy operability, especially for the alignment of the windows to the nanostructures, for sizes of the membrane windows around 5 × 5 mm. Membranes larger than 10 × 10 mm already showed significant instability and easy fracture even during simple cleaning steps. The described fabrication method can be easily transferred to monocrystalline diamond and adjusted for various applications and structures, e.g. photonic crystals for quantum information technologies.

Fluorescence mapping was used to investigate the optical properties of the fabricated NCD nanopillar arrays and the substrate membrane with a confocal microscope. Typical fluorescence maps are shown in **Figure 4**, which demonstrate the fluorescence intensities of the pillars depending on the focal plane along the z-axis of the structures.

Bright spots can be distinguished for individual pillars with intensities ranging from 3 to 6 Mcps, demonstrating similar fluorescence intensities compared to pillars from an earlier study,[22] fabricated in a similar manner, using the same deposition system, parameters, and structuring conditions. The fluorescence intensities at the edge of an array were slightly higher compared to pillars at the center due to the already mentioned slightly different shape (more tapered) of the pillars at the rim of an array. When the focal plane of the confocal microscope was set below the pillars, the background fluorescence of the membrane had a lower intensity in the range of 2.5 Mcps. The photoluminescence (PL) spectra taken from the structures at room temperature showed broad peaks in the wavelength range of 735–743 nm which can be attributed to the zero-phonon line of SiV centers (**Figure 5**). The large spread of the peaks may be explained by ensembles of SiV centers and variable stress in individual diamond grains.[36] They stem from

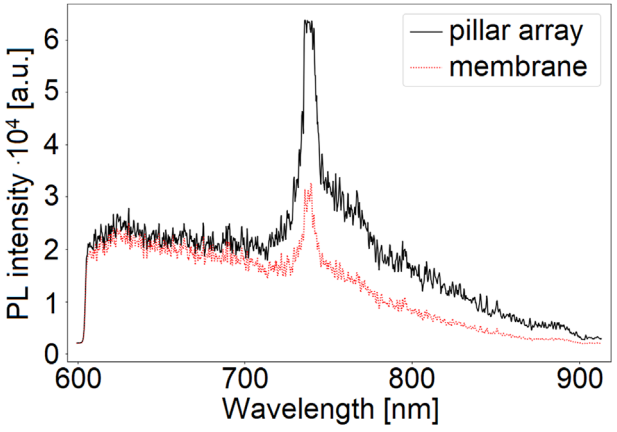

Figure 5. Room temperature PL spectra taken from a diamond nanopillar array (black) and from the "bulk" membrane (red).

Si atoms etched from the substrate and incorporated in the growing NCD films. The intensity of the PL signal taken from the nanopillar arrays was higher compared to the signal from the "bulk" membrane which could be attributed to an enhanced photon collection.

3. Conclusion

We have implemented a fabrication process of highly dense arrays of nanopillars on a NCD membrane by means of EBL, RIE with oxygen plasma and anisotropic wet etching in KOH. Additionally, a completely etched marker hole in the center of the pillar array was structured, which can function as an alignment marker for a deterministic single ion implantation into the pillars for the generation of color centers (single or ensembles). Fluorescence maps indicated the enhanced photon collection efficiency and therefore higher fluorescence intensities out of the nanopillars compared to the unstructured membrane material. The PL spectra revealed the presence of SiV centers incorporated in the NCD films during their growth. Upon integration of ensembles or single NV or SiV centers, such nanostructures fabricated in monocrystalline diamond can play an important role for the development of novel and scalable quantum components and devices.

4. Experimental Section

Diamond Film Deposition: NCD films were grown in a self-built hot filament chemical vapor deposition (HFCVD) system using a gas mixture of 1% CH_4 in H_2 with a total gas flow of 505 sccm. The setup features seven tungsten filaments providing quite homogeneous deposition on three-inch wafers. Detailed information about the setup can be found in Ref. [37]. The other main growth parameters were as following: substrate temperature ca. 890 °C, filament temperature ca. 2000 °C, and working pressure 25 mbar. (100) silicon wafers were utilized as substrates, which were sonicated in a suspension of diamond powders of different sizes in n-pentane to create a nucleation density of about 1×10^{10} cm^{-2}.[38] Typical NCD films with a thickness of ca. 600 nm (after 3 h deposition) were closed and showed well-facetted topography with crystallite sizes in the range of a few hundreds of nm at most. They were thoroughly characterized in an earlier work by scanning electron microscopy (SEM), X-ray diffraction, X-ray photo-electron spectroscopy, and Raman spectroscopy.[37] The initial thickness of the films investigated in the current study was ca. 3 µm (after 9 h deposition), showing crystallite sizes up to 1 µm. The final membrane thickness was around 1.5 µm after planarization and pillar structuring.

Planarization of the Diamond Films: The relatively high surface roughness of the diamond film was reduced by a planarization process. The planarization process reported in ref. [39] had to be expanded to achieve the typical root mean square roughness values of ca. 6 nm, because of the much higher initial surface roughness of the thicker NCD films. The process started with the spin-coating of a spin-on-glass (SOG) (20 wt% perhydropolysilazane (PHPS) in *n*-dibutylether, NN120-20, durXtreme). Subsequent heating at 180 °C for 1 h on a hot plate led to the formation of an amorphous silica-like layer with a very smooth surface, which was transferred to the diamond surface by ICP RIE (Oxford Plasmalab 1000). The main process parameters were as follows: no ICP power, RF power of 250 W, O_2 flow of 23 sccm, SF_6 flow of 2 sccm, working pressure of 5 mTorr and substrate temperature of 30 °C. The etch duration was increased from 8 min to 12 min and the complete process was repeated for another 12 min of dry etching. During the etching the substrate temperature was kept constant with the help of a controlled table and He-backing. This planarization led to the removal of ca. 700 nm of the initial diamond film thickness resulting in a typical root mean square roughness of about 6 nm.

Structuring of NCD Nanopillars Integrated on a Membrane: After planarization the ca. 2.3 µm thick diamond films were structured by EBL and RIE. The full structuring process consisted of two successively aligned electron beam lithographies (Raith eline) and one conventional lithography aligned from the backside of the samples (see Figure 1). Before patterning, the back side of the samples was coated with a 600 nm thick NCD film deposited under the conditions mentioned above for later backside structuring (Figure 1a).

The first EBL started with the spin-coating of a negative e-beam resist (AR-N 7520.18, Allresist) on top of the planarized diamond film. Round features (for the hole markers) with diameters of 2 µm were written by EBL. After the resist development, a hard mask of 200 nm aluminum was deposited by electron beam evaporation (Pfeiffer PLS 500), followed by a lift-off process immersing the samples in 1-methyl-2-pyrrolidone (NMP) at 80 °C (Figure 1b). The round features were transferred into the diamond film by ICP RIE (Oxford Plasmalab 1000) using the following recipe: ICP power 1000 W, RF power 200 W, O_2 flow 10 sccm, working pressure 5 mTorr, substrate temperature 30 °C, and an etch duration of 25 min to etch the hole markers completely through the diamond film with typical etch rates of ca. 100 nm min^{-1} (Figure 1c). The remaining aluminum mask was removed by an aluminum etchant consisting of phosphoric acid, nitric acid, acetic acid and water (H_3PO_4:HNO_3:CH_3COOH:H_2O = 80%:5%:5%:10%), followed by cleaning in acetone and isopropanol.

The second EBL was aligned around the previously structured holes, using a positive resist (AR-P 617.06, Allresist), defining arrays of round features with a diameter of 200 nm and a center-to-center distance of 400 nm (Figure 1d). The pattern design was written with a base exposure dose of 21 µC cm^{-2} and proximity correction software (Figure 3d, Raith eline software) was used to calculate individual exposure dose factors for each pillar feature depending on its position in the array to compensate the typical underexposure at the edge of the array, resulting in unevenly shaped nanopillars and varying diameters. Following the same procedure as in the first EBL, 200 nm aluminum was applied as a hard mask (Figure 1e), followed by an ICP RIE step with the above mentioned conditions. An etch duration of 8 min led to the formation of nanopillars with a height of ca. 800 nm (Figure 1f) and final diamond film thickness of ca. 1.5 µm.

After the complete structuring of the nanopillars, large windows (ca. 5 × 6 mm) were opened into the NCD film on the backside of the sample by lithography and dry etching (Figure 1g). Therefore, the backside was masked off with adhesive tape aligned to the structured spots of the top side, followed by deposition of 200 nm aluminum as a hard mask, which was structured by a mechanical lift-off. After removal of the adhesive tape and the aluminum film on top of it, the window in the aluminum mask was transferred into the NCD by ICP RIE as described before. Subsequently, anisotropic wet etching in 44 % KOH at 85 °C was used to remove the silicon in the exposed windows from the backside of the samples, suspending the structured NCD film into air (Figure 1 and 2a).

Characterization of the Nanopillar Arrays: The morphology, the quality and the size of the structured nanopillars and holes were investigated by SEM (Hitachi S-4000). The optical characterizations were performed with a home-built confocal microscope. An oil immersion objective (Leica HCX PL APO 100x, NA = 0.7–1.4) was applied which was set to NA = 1.4. The observations were made using a standard #1.5 (≈0.17 mm thick) glass coverslip. The pinhole for the confocal detection was a multimode fiber with a core diameter of 50 µm (NA = 0.22). A frequency-doubled Nd:YAG laser (CNI Laser MGL III-532) was implemented as an excitation light source at 532 nm with 250 µW of optical power shone into the objective. The excitation beam size was set in a way that the $1/e^2$-radius equaled the pupil size. A single photon avalanche detector with high quantum efficiency and low dark count (LaserComponents Count-50 SPAD) was applied for the photon detection. Room temperature photoluminescence spectra were measured using a spectrograph Andor Chymera 193i with a

300 line mm^{-1} grating coupled to an Andor iDus DU416A CCD detector. The spectra were measured with a long pass filter with a cutoff around 605 nm.

Acknowledgements

The authors gratefully acknowledge the Volkswagen Foundation (Volkswagen Stiftung) for the financial support under the project "Quantum Coins and Nano Sensors" (Az. 91 000 and 91 001).

Conflict of Interest

The authors declare no conflict of interest.

Keywords

color centers, electron beam lithography, nanocrystalline diamond membranes, nanopillars

Received: March 29, 2019
Revised: April 26, 2019
Published online: May 28, 2019

[1] A. A. Bukach, S. Y. Kilin, *Opt. Spectrosc.* **2007**, *103*, 202.
[2] C.-H. Su, A. D. Greentree, L. C. L. Hollenberg, *Phys. Rev. A* **2009**, *80*, 523081.
[3] I. Aharonovich, S. Castelletto, D. A. Simpson, C.-H. Su, A. D. Greentree, S. Prawer, *Rep. Prog. Phys.* **2011**, *74*, 76501.
[4] V. Acosta, P. Hemmer, *MRS Bull.* **2013**, *38*, 127.
[5] M. V. Dutt, L. Childress, L. Jiang, E. Togan, J. Maze, F. Jelezko, A. S. Zibrov, P. R. Hemmer, M. D. Lukin, *Science* **2007**, *316*, 1312.
[6] G. Balasubramanian, P. Neumann, D. Twitchen, M. Markham, R. Kolesov, N. Mizuochi, J. Isoya, J. Achard, J. Beck, J. Tissler, V. Jacques, P. R. Hemmer, F. Jelezko, J. Wrachtrup, *Nat. Mater.* **2009**, *8*, 383.
[7] A. Faraon, C. Santori, Z. Huang, V. M. Acosta, R. G. Beausoleil, *Phys. Rev. Lett.* **2012**, *109*, 033604.
[8] H. Sternschulte, K. Thonke, R. Sauer, P. C. Münzinger, P. Michler, *Phys. Rev. B* **1994**, *50*, 14554.
[9] B. J. M. Hausmann, M. Khan, Y. Zhang, T. M. Babinec, K. Martinick, M. McCutcheon, P. R. Hemmer, M. Loncar, *Diamond Relat. Mater.* **2010**, *19*, 621.
[10] C. J. Widmann, C. Giese, M. Wolfer, D. Brink, N. Heidrich, C. E. Nebel, *Diamond Relat. Mater.* **2015**, *54*, 2.
[11] A. E. Rugar, C. Dory, S. Sun, J. Vučković, **2018**, arXiv:1811.09941 [quant-ph].
[12] J. L. Zhang, K. G. Lagoudakis, Y.-K. Tzeng, C. Dory, M. Radulaski, Y. Kelaita, K. A. Fischer, S. Sun, Z.-X. Shen, N. A. Melosh, S. Chu, J. Vučković, *Optica* **2017**, *4*, 1317.
[13] J. Riedrich-Möller, L. Kipfstuhl, C. Hepp, E. Neu, C. Pauly, F. Mücklich, A. Baur, M. Wandt, S. Wolff, M. Fischer, S. Gsell, M. Schreck, C. Becher, *Nat. Nanotechnol.* **2012**, *7*, 69.
[14] A. Faraon, P. E. Barclay, C. Santori, K. M. C. Fu, R. G. Beausoleil, *Nat. Photonics* **2011**, *5*, 301.
[15] B. Khanaliloo, M. Mitchell, A. C. Hryciw, P. E. Barclay, *Nano Lett.* **2015**, *15*, 5131.
[16] J. L. Zhang, S. Sun, M. J. Burek, C. Dory, Y.-K. Tzeng, K. A. Fischer, Y. Kelaita, K. G. Lagoudakis, M. Radulaski, Z.-X. Shen, N. A. Melosh, S. Chu, M. Lončar, J. Vučković, *Nano Lett.* **2018**, *18*, 1360.
[17] I. Aharonovich, C. Santori, B. A. Fairchild, J. Orwa, K. Ganesan, K.-M. C. Fu, R. G. Beausoleil, A. D. Greentree, S. Prawer, *J. Appl. Phys.* **2009**, *106*, 124904.
[18] B. Naydenov, V. Richter, J. Beck, M. Steiner, P. Neumann, G. Balasubramanian, J. Achard, F. Jelezko, J. Wrachtrup, R. Kalish, *Appl. Phys. Lett.* **2010**, *96*, 163108.
[19] R. E. Evans, A. Sipahigil, D. D. Sukachev, A. S. Zibrov, M. D. Lukin, *Phys. Rev. Appl.* **2016**, *5*, 044010.
[20] V. Sedov, V. Ralchenko, A. A. Khomich, I. Vlasov, A. Vul, S. Savin, A. Goryachev, V. Konov, *Diamond Relat. Mater.* **2015**, *56*, 23.
[21] K. Ohno, F. J. Heremans, L. C. Bassett, B. A. Myers, D. M. Toyli, A. C. Bleszynski Jayich, C. J. Palmstrom, D. D. Awschalom, *Appl. Phys. Lett.* **2012**, *101*, 082413.
[22] E. Petkov, T. Rendler, C. Petkov, F. Schnabel, J. P. Reithmaier, J. Wrachtrup, C. Popov, W. Kulisch, *Phys. Status Solidi A* **2013**, *210*.
[23] N. Felgen, B. Naydenov, S. Turner, F. Jelezko, J. P. Reithmaier, C. Popov, *Diamond Relat. Mater.* **2016**, *64*, 64.
[24] J. Meijer, T. Vogel, B. Burchard, I. W. Rangelow, L. Bischoff, J. Wrachtrup, M. Domhan, F. Jelezko, W. Schnitzler, S. A. Schulz, K. Singer, F. Schmidt-Kaler, *Appl. Phys. A* **2006**, *83*, 321.
[25] J. L. Pacheco, M. Singh, D. L. Perry, J. R. Wendt, G. Ten Eyck, R. P. Manginell, T. Pluym, D. R. Luhman, M. P. Lilly, M. S. Carroll, E. Bielejec, *Rev. Sci. Instrum.* **2017**, *88*, 123301.
[26] G. Jacob, K. Groot-Berning, S. Wolf, S. Ulm, L. Couturier, U. G. Poschinger, F. Schmidt-Kaler, K. Singer, **2014**, arXiv:1405.6480 [physics.atom-ph].
[27] K. Groot-Berning, T. Kornher, G. Jacob, F. Stopp, S. T. Dawkins, R. Kolesov, J. Wrachtrup, K. Singer, F. Schmidt-Kaler, **2019**, arXiv:1902.05308 [quant-ph].
[28] A. P. Magyar, J. C. Lee, A. M. Limarga, I. Aharonovich, F. Rol, D. R. Clarke, M. Huang, E. L. Hu, *Appl. Phys. Lett.* **2011**, *99*, 081913.
[29] A. H. Piracha, K. Ganesan, D. W. M. Lau, A. Stacey, L. P. McGuinness, S. Tomljenovic-Hanic, S. Prawer, *Nanoscale* **2016**, *8*, 6860.
[30] K. Bray, B. Regan, A. Trycz, R. Previdi, G. Seniutinas, K. Ganesan, M. Kianinia, S. Kim, I. Aharonovich, *ACS Photonics* **2018**, *5*, 4817.
[31] A. Faraon, P. E. Barclay, C. Santori, K.-M. C. Fu, R. G. Beausoleil, *Nat. Photonics* **2011**, *5*, 301.
[32] P. Maletinsky, S. Hong, M. S. Grinolds, B. Hausmann, M. D. Lukin, R. L. Walsworth, M. Loncar, A. Yacoby, *Nat. Nanotechnol.* **2012**, *7*, 320.
[33] P. Ovartchaiyapong, L. M. A. Pascal, B. A. Myers, P. Lauria, A. C. Bleszynski Jayich, *Appl. Phys. Lett.* **2012**, *101*, 163505.
[34] S. Cui, X. Zhang, T. Liu, J. Lee, D. Bracher, K. Ohno, D. Awschalom, E. L. Hu, *ACS Photonics* **2015**, *2*, 465.
[35] L. Ondic, M. Varga, K. Hruska, J. Fait, P. Kapusta, *ACS Nano* **2017**, *11*, 2972.
[36] I. Aharonovich, E. Neu, *Adv. Optical Mater.* **2014**, *2*, 911.
[37] W. Kulisch, C. Petkov, E. Petkov, C. Popov, P. N. Gibson, M. Veres, R. Merz, B. Merz, J. P. Reithmaier, *Phys. Status Solidi A* **2012**, *209*, 1664.
[38] W. Kulisch, C. Popov, T. Sasaki, L. Sirghi, H. Rauscher, F. Rossi, J. P. Reithmaier, *Phys. Status Solidi A* **2011**, *208*, 70.
[39] N. Felgen, A. Schmidt, B. Naydenov, J. Jelezko, J. P. Reithmaier, C. Popov, *Advanced Nanotechnologies for Detection and Defence against CBRN Agents. NATO Science for Peace and Security Series B: Physics and Biophysics*. (Eds: P. Petkov, D. Tsiulyanu, C. Popov, W. Kulisch), Springer, Dordrecht **2018**, Ch. 19.7.